Electron carrier concentration dependent magnetization and transport properties in ZnO:Co diluted magnetic semiconductor thin films

Z. Yang,[1] M. Biasini,[2] W. P. Beyermann,[2] M. B. Katz,[3] O. K. Ezekoye,[3] X. Q. Pan,[3] Y. Pu,[2] J. Shi,[2] Z. Zuo,[1] and J. L. Liu[1,a)]
[1]*Department of Electrical Engineering, Quantum Structures Laboratory, University of California, Riverside, California 92521, USA*
[2]*Department of Physics and Astronomy, University of California, Riverside, California 92521, USA*
[3]*Department of Materials Science and Engineering, University of Michigan, Ann Arbor, Michigan 48109, USA*

(Received 18 August 2008; accepted 14 October 2008; published online 4 December 2008)

Diluted magnetic semiconducting ZnO:Co thin films with above room-temperature T_C were prepared. Transmission electron microscopy and x-ray diffraction studies indicate the ZnO:Co thin films are free of secondary phases. The magnetization of the ZnO:Co thin films shows a free electron carrier concentration dependence, which increases dramatically when the free electron carrier concentration exceeds $\sim 10^{19}$ cm^{-3}, indicating a carrier-mediated mechanism for ferromagnetism. The anomalous Hall effect is observed in the ZnO:Co thin films. The anomalous Hall coefficient and its dependence on longitudinal resistivity were analyzed. The presence of a side-jump contribution further supports an intrinsic origin for ferromagnetism in ZnO:Co thin films. These observations together with the magnetic anisotropy and magnetoresistance results support an intrinsic carrier-mediated mechanism for ferromagnetic exchange in ZnO:Co diluted magnetic semiconductor materials. © *2008 American Institute of Physics*. [DOI: 10.1063/1.3033402]

I. INTRODUCTION

Diluted magnetic semiconductor (DMS) (Ref. 1) materials have been widely studied because of their potential applications in spintronics.[2–7] In the last two decades, rapid and outstanding progress was achieved in several group II–VI and III–V DMS materials, such as Mn-doped ZnSe,[1,3] GaAs,[2,4] and InAs.[5,6] The origin and mechanism of ferromagnetism in these DMS materials have been well studied and are believed to be free-carrier mediated exchange between magnetic ions. However, the Curie temperatures (T_C) of these DMS materials are all far below the room temperature, which hinders their applications in commercial products. In recent years, magnetically doped ZnO has emerged as a possible DMS material,[8,9] because theoretical calculations have predicted an above room-temperature T_C.[10,11] However, experimental results on ZnO-based materials are still controversial.[8,12–25] In addition to ferromagnetism,[12–20] nonferromagnetic states,[21–25] such as spin-glass,[21] antiferromagnetism,[22] and paramagnetism,[23] have also been reported. Furthermore, the origin of the ferromagnetism in ZnO-based DMS materials is still controversial, unlike the DMS materials mentioned above such as GaAs:Mn. Some researchers reported clustering or secondary phase formation as the origin of the ferromagnetism (i.e., an extrinsic mechanism),[26–28] while others concluded that an intrinsic carrier-mediated mechanism was responsible for the ferromagnetism.[29–31] In order to experimentally investigate and prove the presence of intrinsic carrier-mediated ferromagnetism in ZnO, some advanced experiments have been recently designed. For example, studies on ZnO codoped with a transition metal and either a donor or acceptor dopant, such as Zn interstitials,[32–35] Al,[36–39] and Ga (Ref. 40) for *n*-type conduction and N,[41–44] P,[45,46] and As (Refs. 47 and 48) for *p*-type conduction, have been pursued to check the role of the free carriers in the ferromagnetism in ZnO-based DMS materials. Furthermore, electrical transport and optical probes beyond the more common techniques for studying magnetism (e.g., bulk magnetization), such as anomalous Hall effect (AHE) (Refs. 49–53) and magnetic circular dichroism,[7] were performed on ZnO-based DMS materials to help distinguish between intrinsic and extrinsic mechanisms of ferromagnetism. In this paper, we report results on the free electron carrier concentration dependence of the magnetization, AHE, magnetoresistance (MR), magnetic anisotropy, and transmission electron microscopy (TEM) studies on ZnO:Co thin films. These experimental data provide strong evidence in support of intrinsic carrier-mediated ferromagnetism in ZnO DMS materials.

II. EXPERIMENT

The ZnO and ZnO:Ga thin films were grown on *r*-cut sapphire substrates using plasma-assisted molecular-beam epitaxy. Regular effusion cells filled with elemental Zn (6*N*) and Ga (6*N*) were used as zinc and gallium sources. Radio frequency plasma supplied with O_2 (5*N*) was used as the oxygen source. The electron carrier concentration of the ZnO:Ga thin films was tuned by the amount of Ga incorporation, which was controlled by the Ga effusion cell temperature. The substrate temperature was kept at 565 °C during the growth. After growth, the samples were annealed *in situ* in vacuum at 800 °C for 20 min to activate the Ga dopants

a)Author to whom correspondence should be addressed. Electronic mail: jianlin@ee.ucr.edu.

TABLE I. Electron carrier concentrations before and after implantation and the saturated magnetization of ZnO:Co thin film samples. The data were taken at room temperature. Note that μ_B stands for the Bohr magneton.

Sample no.	Electron concentration before implantation n_0 (cm^{-3})	Electron concentration after implantation n (cm^{-3})	Saturated magnetization M_S (μ_B per Co ion)
A	1.2×10^{20}	8.3×10^{19}	4.6
B	3.4×10^{19}	3.6×10^{19}	4.1
C	8.4×10^{18}	4.0×10^{18}	1.4
D	3.5×10^{18}	1.3×10^{18}	0.3
E	4.7×10^{19}	2.8×10^{19}	4.1

and improve crystallinity. The electron carrier concentration values of these ZnO and ZnO:Ga samples are shown in Table I as "before implantation" carrier concentration n_0. More detailed information on ZnO:Ga samples can be found elsewhere.[54]

The Co ions were implanted into as-grown ZnO and ZnO:Ga thin films with a dose of 3×10^{16} cm^{-2} and an implantation energy of 50 keV. The total amount of Co ions implanted in each ZnO film was calculated by the dose and area of the sample. All Co-implanted ZnO samples were annealed at 900 °C for 5 min in nitrogen after implantation to activate the implanted Co ions and recover the crystallinity. (In the context of this paper, both ZnO and ZnO:Ga thin films are referred to ZnO samples for convenience, since Ga doping is only used to tune the electron carrier concentration of the ZnO thin films, and ZnO:Co represent samples implanted with Co ions and annealed using the above mentioned procedure. All the experiments, such as magnetic and transport properties measurements, were performed on the annealed samples.) The electron carrier concentrations of the ZnO:Co samples were shown in Table I as "after implantation" carrier concentration n.

Figure 1 shows secondary ion mass spectroscopy (SIMS) spectra of (a) the ZnO thin film before Co ion implantation, (b) the ZnO:Co thin film immediately after the implantation but before annealing, and (c) the ZnO:Co thin film after implantation and annealing at 900 °C for 5 min. As shown in Fig. 1(a), the Zn and Ga distributions are fairly uniform throughout the depth of the ZnO film. After Co implantation, the implanted Co ion concentration follows a Gaussian distribution with a peak near the surface of the ZnO:Co thin film as shown in Fig. 1(b). The fact that the Gaussian peak is near the surface is an intentional result of a low implantation energy intended to prevent a significant amount of Co ions from reaching the sapphire substrate. After annealing at 900 °C for 5 min, the Co ions redistribute to a relatively uniform profile along the depth of the ZnO:Co film as shown in Fig. 1(c). Ga atoms are piling near the ZnO/sapphire interface shown in Fig. 1(c), which is possibly due to the migration of the Ga atoms after high temperature annealing. Although most of the Co ions are in the ZnO film layer, a tiny amount of residual Co ions may have reached the sapphire substrate region for both unannealed and annealed samples; however, their concentrations are more than one order of magnitude smaller than the Co ion concentrations in the ZnO films. Any magnetic contribution from the substrates was removed from the magnetization data with the following procedure. We first measured the ZnO:Co thin film on the sapphire substrate. Then we completely etched away the ZnO:Co layer using diluted hydrochloric acid and measured just the sapphire substrate. The magnetic response of the ZnO:Co thin films was obtained by subtracting the two data sets. The magnetization data of the ZnO:Co thin films discussed in this paper all followed this procedure.

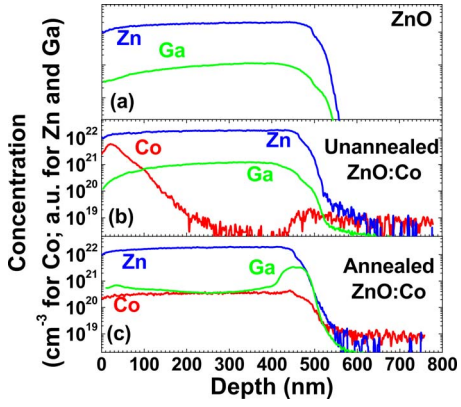

FIG. 1. (Color online) SIMS spectra for (a) the as-grown ZnO thin film, (b) the ZnO:Co thin film after Co ion implantation, but before annealing, and (c) the ZnO:Co thin film after annealing at 900 °C for 5 min (sample A). The magnetic measurements were all performed on the annealed samples.

TEM studies were carried out on a JEOL JEM 3011 high resolution electron microscope operated at 300 kV, with a point-to-point resolution of 0.17 nm. Cross-sectional TEM specimens were prepared via mechanical grinding, polishing, and dimpling, followed by argon ion milling in a Gatan model 691 precision ion polishing system at incident angles between 4° and 5.5° to electron transparency. X-ray diffraction (XRD) measurements were performed using a Bruker D8 Advance x-ray diffractometer. Magnetic properties were measured with a Quantum Design MPMS-XL superconducting quantum interference device (SQUID) magnetometer using an in-plane geometry (magnetic field parallel to the film) on all samples unless specified differently. MR and field-dependent Hall effect measurements were performed with Hall bar geometry using a Quantum Design PPMS equipment. The magnetic field was perpendicular to the film plane of the samples in the MR measurements. In addition to field-dependent Hall effect measurements, the ordinary Hall effect (OHE) measurements were also carried out separately with Van der Pauw geometry using an Ecopia HMS-3000 room-temperature Hall effect system at constant magnetic field of 1 T to get the electron carrier concentration of the samples. SIMS measurements were performed using a PHI ADEPT-1010 Dynamic SIMS system.

III. RESULTS AND DISCUSSION

A. Structural properties

Figure 2(a) shows a cross-sectional TEM image of a typical ZnO:Co thin film on an *r*-cut sapphire substrate (sample A). The TEM image shows a relatively low disloca-

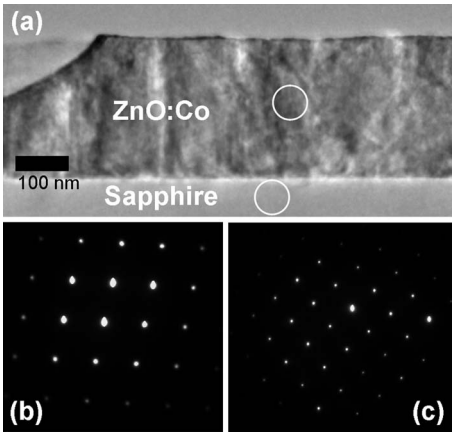

FIG. 2. (a) Cross-sectional TEM image of a ZnO:Co thin film on a sapphire substrate (sample A). SAED patterns of (b) ZnO:Co thin film and (c) sapphire substrate, taken from the areas indicated by the white circles.

tion density, indicating a high quality film. Selected area electron diffraction (SAED) patterns from the areas indicated by the white circles in Fig. 2(a) are shown in Fig. 2(b) for the ZnO:Co thin film and in Fig. 2(c) for the sapphire substrate. Similar SAED patterns were observed from various different positions along the film. These diffraction patterns are symmetric and uniform, indicating the absence of clustering and secondary phase formation.

Figures 3(a) and 3(b) show typical high resolution TEM (HRTEM) images of the film/substrate interface and the film itself, respectively. The zone axes of the film and the substrate are approximately 3° apart from each other, indicating a slight twist between the film and the substrate. The crystallographic alignment of the ZnO:Co layer with the sapphire substrate at the interface is good. HRTEM studies indicate that the film is of high crystallinity, and no clustering or secondary phases were observed; however, a small number of stacking faults were observed.

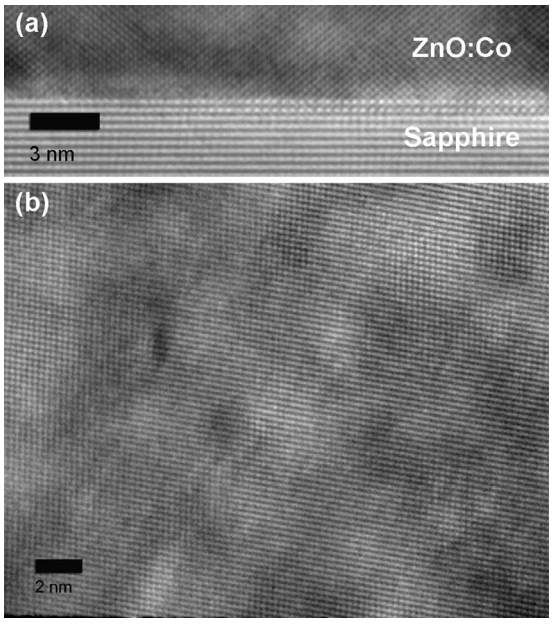

FIG. 3. (a) Cross-sectional HRTEM image of the interface between the ZnO:Co thin film and the sapphire substrate in sample A, showing an atomically sharp interface. (b) HRTEM image of the ZnO:Co thin film (sample A). The film has high crystallinity with no observable secondary phase.

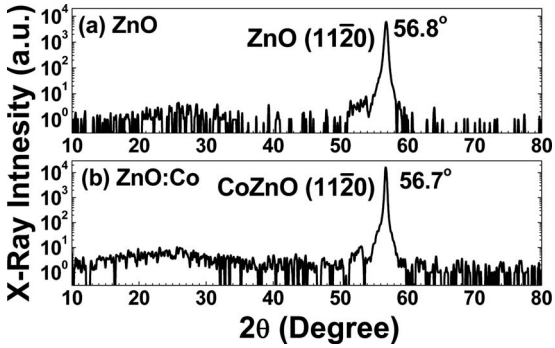

FIG. 4. XRD spectra of (a) ZnO and (b) ZnO:Co thin films (sample A). Both the ZnO and ZnO:Co thin films show high crystallinity with no impurity phases within the detection limit of the system.

Figures 4(a) and 4(b) show XRD patterns of typical ZnO and ZnO:Co thin films (sample A). The only ZnO (11$\bar{2}$0) peak, which was observed at approximately 56.8°, did not show any significant change after Co implantation, indicating the Co implantation did not significantly degrade the sample's crystallinity. Furthermore, no Co-related impurity phase or compound peaks were detected in the XRD pattern in Fig. 4(b) within the detection limit of the system.

B. Magnetic properties

Figure 5(a) shows the magnetic field dependence of the magnetization (M-H) of a ZnO:Co thin film (sample A) at a temperature of 300 K. The M-H curve measured at 10 K is shown in the inset. The saturated magnetization M_S value is approximately $4.6\mu_B$ per Co ion, which is larger than most of previously reported values,[31,32,37,39,41,55–57] but it is smaller than the giant magnetic moments observed in ZnO:Co (6.1 and $18.9\mu_B$ per Co)[58,59] and SnO_2:Co thin films ($7.5\pm0.5\mu_B$ per Co).[60] For metallic Co, the saturated magnetization is around $1.7\mu_B$ per Co, a consequence of band ferromagnetism. The value we measured for this ZnO:Co thin film is midway between that calculated for isolated divalent Co ions with full angular momentum (i.e., $gJ=6\mu_B$) and that calculated with the orbital angular momentum quenched (i.e., $2S=3\mu_B$), suggesting that the ferromagnetism of the samples is not from the metallic Co clusters. This is consistent with the HRTEM analyses and XRD data. The temperature dependence of the magnetization, measured with a magnetic field of 0.2 T, of the ZnO:Co thin film (sample A) is shown in Fig. 5(b). The standard sample insert was used to measure the magnetization from 2 to 350 K, while an oven insert with a brass sample holder was used for the measurements from 300 to 800 K. A more restricted sample enclosure resulted in noisier data at high temperature. The Curie temperature is above the upper-temperature limit of the system (800 K). Using the approximate relation $M=M_0(T_C-T)^{1/2}$, the data were extrapolated to obtain an estimate for the Curie temperature of ~950 K. The field dependence of the magnetization of this sample measured at 700 K is shown in the inset of Fig. 5(b).

ZnO:Co thin film samples with different electron carrier concentrations, ranging from 1.3×10^{18} to 8.3×10^{19} cm^{-3}, were prepared to investigate the electron carrier concentra-

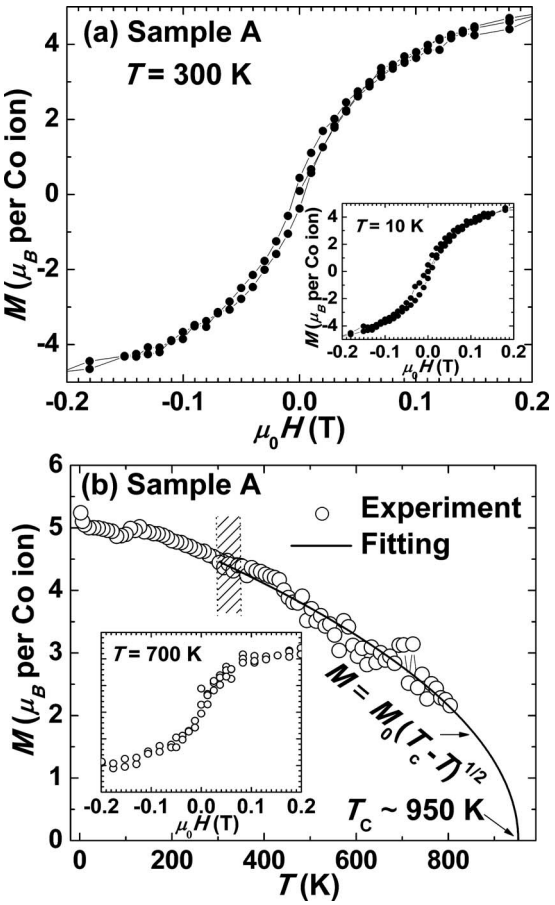

FIG. 5. (a) The magnetic field dependence of the magnetization for a ZnO:Co thin film (sample A) measured at 300 and 10 K (inset). (b) The temperature dependence of the saturated magnetization, from 2 to 800 K measured with an applied field of 0.2 T. A high temperature extrapolation of the data indicates that the Curie temperature is around 950 K. The inset shows the field dependence of the magnetization of this sample measured at 700 K.

tion dependence of magnetization. Figure 6(a) shows the ferromagnetic hysteresis loops for ZnO:Co thin films B, C, and D measured at 300 K. The saturated magnetization of sample B ($4.1\mu_B$ per Co) is slightly smaller than sample A ($4.6\mu_B$ per Co) in Fig. 5(a). However, when the electron carrier concentration decreases below $\sim 10^{19}$ cm^{-3} as in samples C and D, the saturated magnetizations drop dramatically to 1.4 and $0.3\mu_B$ per Co, respectively. The carrier concentrations, measured both before and after Co ion implantation, and the saturated magnetization are listed in Table I for the ZnO:Co thin film samples. Figure 6(b) shows the experimental relation between the saturated magnetization (M_S) and the free electron carrier concentration (n) measured after Co ion implantation in samples A-E. A polynomial fit (dashed line) to the experimental data (open circles) provides a guide for the eyes, although the physical meaning behind this trend needs further clarification.

Figure 7 shows the anisotropic magnetization for ZnO:Co thin film sample E. The out-of-plane (magnetic field perpendicular to the film plane) and in-plane (magnetic field parallel to the film plane) field dependences of the magnetization are shown with open and solid circles in Fig. 7, respectively. The out-of-plane curve shows a weaker magnetization before saturation than the in-plane geometry. The ZnO thin films were epitaxially grown on *r*-cut sapphire substrates with the growth direction along the $[11\bar{2}0]$ direction as indicated by the XRD pattern [Fig. 4(b)]. This result indicates that the easy magnetization axis is in the plane of the film, which is consistent with similar magnetic anisotropy experiments on ZnO:Co thin films reported by other groups.[57] Magnetic anisotropy is further evidence for an intrinsic nature of the ferromagnetism in ZnO:Co DMS thin films[56,57] since the cluster-related ferromagnetism is generally isotropic.

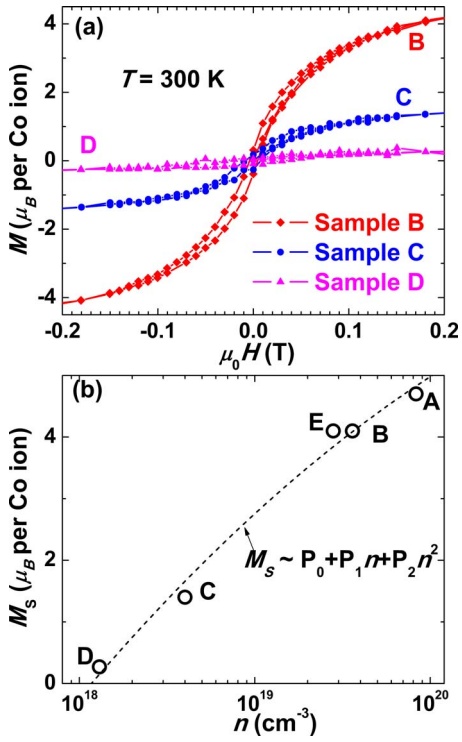

FIG. 6. (Color online) (a) The magnetic field dependence of the magnetization for ZnO:Co thin film samples B, C, and D measured at a temperature of 300 K. (b) The dependence of the saturated magnetization M_S on electron carrier concentration n in ZnO:Co thin film samples. A polynomial fitting to the data is indicated with the dashed line.

C. Transport properties

Figure 8(a) shows the transverse MR, MR$=[R(\mu_0 H) - R(0)]/R(0)$, for ZnO:Co thin film sample E measured at the

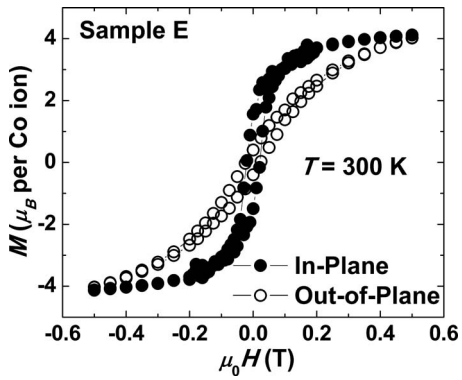

FIG. 7. Magnetic anisotropy of a ZnO:Co thin film (sample E) measured at a temperature of 300 K. The in-plane field dependence of the magnetization (solid circles) is stronger than out-of-plane magnetization (open circles).

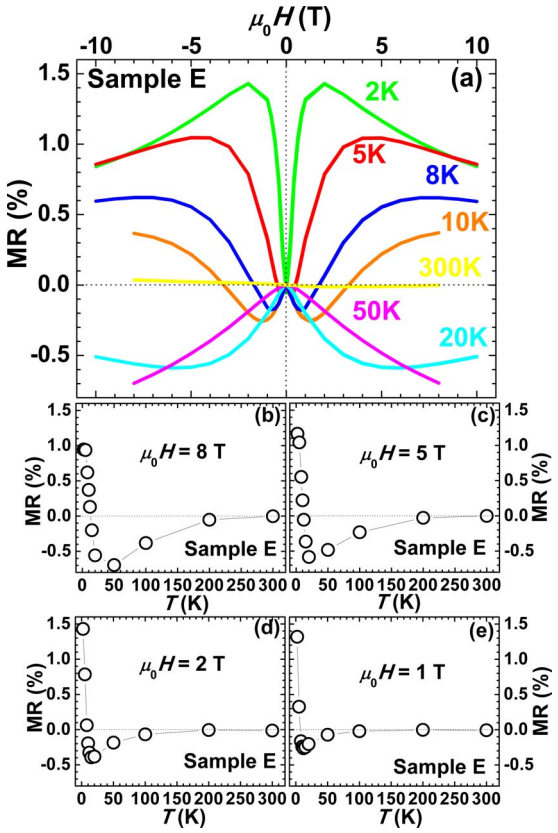

FIG. 8. (Color online) (a) Transverse MR, MR=$[R(H)-R(0)]/R(0)$, of a ZnO:Co thin film (sample E) measured at different temperatures from 2 to 300 K. The applied magnetic field was perpendicular to the plane of the film. [(b)–(e)] The temperature dependence of the MR at different magnetic fields of 8, 5, 2, and 1 T.

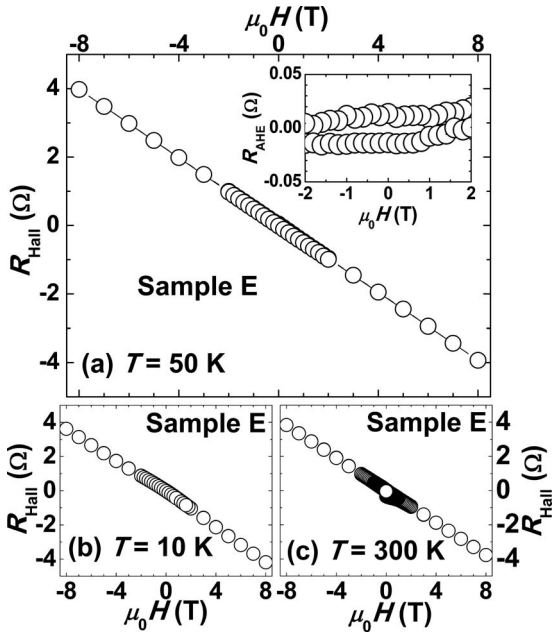

FIG. 9. (a) The Hall resistance as a function of the applied magnetic field for a ZnO:Co thin film (sample E) measured at a temperature of 50 K. The inset shows the AHE data over an expended field range near the origin after the linear OHE contribution was subtracted. [(b)–(c)] The Hall resistance as a function of the applied magnetic field for the same ZnO:Co thin film sample measured at the temperatures of 10 and 300 K.

temperatures of 2, 5, 8, 10, 20, 50, and 300 K. The MR, which measured up to 10 T, in our ZnO:Co thin film is strongly temperature dependent with a positive magnitude from 2 to 5 K and a negative magnitude above 20 K. Between 5 and 20 K, the MR starts out negative and eventually swings positive at higher fields, reflecting competing contributions. A positive MR is attributed to a giant spin splitting of band states caused by a *sp-d* exchange interaction in DMSs.[61–63] A negative MR is from the third-order *sp-d* exchange Hamiltonian of the spin scattering,[64–66] because the second-order theory breaks down at large magnetic fields.[66] Figures 8(b)–8(e) show the temperature dependence of the MR at different magnetic fields of 8, 5, 2, and 1 T, respectively. Furthermore, the MR properties of our ZnO:Co thin films also show carrier-concentration-dependent behavior, in addition to a temperature dependence.[67] We believe the temperature and free carrier concentration dependences of the MR are also a sign of intrinsic carrier mediated ferromagnetism.

Figure 9(a) shows the Hall resistance R_{Hall} as a function of magnetic field for ZnO:Co thin film sample E, measured at a temperature of 50 K. The Hall effect data, measured at 10 and 300 K, are shown in Figs. 9(b) and 9(c). The Hall resistance is the sum of two contributions: the OHE from the classical Lorenz force and the AHE due to an asymmetric scattering in the presence of a magnetization. This is expressed by the equation

$$R_{\mathrm{Hall}} = \frac{R_0}{d}(\mu_0 H) + \frac{R_S}{d}(\mu_0 M) \equiv R_{\mathrm{OHE}} + R_{\mathrm{AHE}}, \tag{1}$$

where the R_{OHE} and R_0 are the ordinary Hall resistance and coefficient, R_{AHE} and R_S are the anomalous Hall resistance and coefficient, and d is the film thickness. H and M are the magnetic field and the magnetization perpendicular to the film plane, and μ_0 is the free space permeability, respectively. In Fig. 9, the Hall resistance data are dominated by a linear contribution with a negative slope from the OHE. The sign and magnitude of the slope provide information on the carrier type and concentration, respectively. The nonlinear component of the Hall resistance is from the AHE. After subtracting the linear background from OHE, the AHE component is shown in the inset in Fig. 9(a). A small amount of hysteresis is observed from the field dependence of M, though the size of the hysteresis loop seems to be larger than that found with magnetization measurements. So far very few AHE results have been reported in ZnO DMS materials,[49–53] and for all these reports, the AHE contributions in ZnO DMS are very small compared to other DMS materials, such as GaAs:Mn (Ref. 2) and GaAs:In (Refs. 5 and 6). Most researchers consider the AHE to be a useful tool for demonstrating the intrinsic nature of ferromagnetic order.[49,52]

The first term in Eq. (1) dominates, but it is possible to determine R_S by extrapolating high-field (>3 T) R_{Hall} data, where M is saturated, back to the origin. The data for R_{Hall}, at positive and negative high fields, were each fit to straight lines. The slopes of these lines correspond to R_0/d. The distance between the two intercepts on the vertical axis is $2R_S\mu_0 M/d$. The ordinary Hall coefficient R_0 and anomalous

TABLE II. The resistivity ρ_{xx}, ordinary Hall coefficient R_0, anomalous Hall coefficient R_S, electron carrier concentration n, and the ratio ρ_{AHE}/ρ_{xx} for ZnO:Co thin film sample E. Data were measured at the temperatures of 10, 50, and 300 K.

T (K)	ρ_{xx} (10^{-3} Ω cm)	R_0 (10^{-5} Ω cm T^{-1})	R_S (10^{-4} Ω cm T^{-1})	n (10^{19} cm^{-3})	ρ_{AHE}/ρ_{xx} (10^{-5})
10	8.62	−2.40	6.3 ± 0.6	2.6	17 ± 2
50	8.49	−2.35	3.4 ± 0.1	2.7	9.2 ± 0.2
300	8.33	−2.26	1.5 ± 0.1	2.8	4.1 ± 0.2

Hall coefficient R_S, determined with this procedure, at 10, 50, and 300 K are listed in Table II. The electron carrier concentration n of this sample at 10, 50, and 300 K were also listed in the table, which were derived from the Hall coefficient R_0 and the relation $n=-1/(eR_0)$. The error bars on R_S come primarily from the high-field extrapolation of data with some experimental noise. The error bars on R_0 are orders of magnitude smaller than the R_0 values. So no error bar for R_0 or n was included in Table II. To our knowledge, we are the first to report R_S for ZnO-based DMS materials. Even though the AHE contribution to the Hall resistance is much smaller than the OHE contribution, R_S for ZnO:Co is large in comparison to values for transition metal ferromagnets.[68] The AHE is difficult to observe in ZnO:Co because the OHE contribution is increased by a small carrier concentration (comparing to metals and III-As:Mn DMS) and the AHE contribution is reduced from a small magnetization per unit volume.

Figure 10 shows the temperature dependence of the resistivity ρ_{xx} of ZnO:Co thin film sample E measured from 2 to 350 K. The ρ_{xx} does not show strong temperature dependence (with orders of magnitude) over the temperature range, because the ZnO:Co thin film is a degenerate semiconductor with this electron carrier concentration. The resistivity values of sample E at 10, 50, and 300 K are also listed in Table II. In general, the anomalous Hall resistivity ρ_{AHE} has both a linear and quadratic dependence on the film resistivity ρ_{xx} as

$$\rho_{AHE} = \phi_{sk}\rho_{xx} + b_{sj}\rho_{xx}^2. \quad (2)$$

The linear term is from skew scattering and the quadratic term originates from a side jump mechanism related to a material's intrinsic properties. The anomalous Hall resistivity ρ_{AHE} is defined as $\rho_{AHE}=(\mu_0 M)R_S$ from $\rho_{Hall}=R_{Hall}d=(\mu_0 H)R_0+(\mu_0 M)R_S \equiv \rho_{OHE}+\rho_{AHE}$, an equivalent equation as Eq. (1), where ρ_{Hall} and ρ_{OHE} are Hall resistivity and ordinary Hall resistivity, respectively. Figure 11 shows ρ_{AHE}/ρ_{xx} versus ρ_{xx}, measured at three temperatures. From a linear fit to the data, $\phi_{sk}=-3.2\times10^{-3}$ and $b_{sj}=0.39\ \Omega^{-1}\ cm^{-1}$. The physical meaning of ϕ_{sk} is the skew scattering angle of a material in radian unit. The negative sign and milliradian magnitude of ϕ_{sk} are common for intrinsic ferromagnetic materials, such as most of the transition metal ferromagnets.[69] The presence of a side-jump contribution further support an intrinsic origin for the ferromagnetism in ZnO:Co thin films.

IV. SUMMARY

In summary, the structural, magnetic, and electrical transport properties of ZnO:Co thin films were comprehensively characterized. No secondary phases were observed by TEM and XRD. Ferromagnetism was observed in ZnO:Co thin films with a Curie temperature far above room temperature. The saturated magnetization of the ZnO:Co thin films increases dramatically when the free electron carrier concentration exceeds $\sim10^{19}$ cm^{-3}, indicating a carrier-mediated mechanism for ferromagnetism. The ZnO:Co thin films show magnetic anisotropy with the easy magnetization axis parallel to the film plane. A strong temperature dependence and competition between positive and negative contributions were observed in MR of the ZnO:Co thin films. Finally, an AHE was observed and analyzed in the ZnO:Co thin films, consistent with long-range ferromagnetism. These experimental results lend support to an intrinsic carrier-mediated mechanism for the ferromagnetic exchange in ZnO:Co DMS materials.

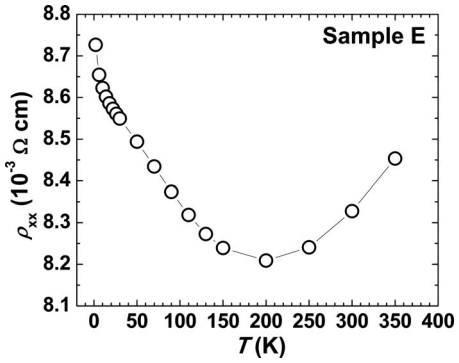

FIG. 10. Temperature dependence of the resistivity of a ZnO:Co thin film (sample E).

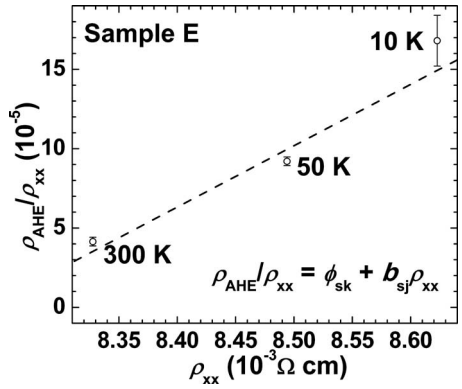

FIG. 11. The ratio of the anomalous Hall resistivity ρ_{AHE} to the resistivity ρ_{xx} as a function of the resistivity ρ_{xx}.

ACKNOWLEDGMENTS

This work was supported by ONR/DMEA through the Center of Nanomaterials and Nanodevices (CNN) under Award No. H94003-08-2-0803. Electron microscopy studies at the Electron Microbeam Analysis Laboratory at the University of Michigan were supported by the National Science Foundation under Grant No. DMR-0315633.

[1] J. K. Furdyna, J. Appl. Phys. **64**, R29 (1988).
[2] H. Ohno, Science **281**, 951 (1998).
[3] R. Fiederling, M. Keim, G. Reuscher, W. Ossau, G. Schmidt, A. Waag, and L. W. Molenkamp, Nature (London) **402**, 787 (1999).
[4] Y. Ohno, D. K. Young, B. Beschoten, F. Matsukura, H. Ohno, and D. D. Awschalom, Nature (London) **402**, 790 (1999).
[5] H. Ohno, D. Chiba, F. Matsukura, T. Omiya, E. Abe, T. Dietl, Y. Ohno, and K. Ohtani, Nature (London) **408**, 944 (2000).
[6] D. Chiba, M. Yamanouchi, F. Matsukura, and H. Ohno, Science **301**, 943 (2003).
[7] K. Ando, Science **312**, 1883 (2006).
[8] C. Liu, F. Yun, and H. Morkoç, J. Mater. Sci. Mater. Electron. **16**, 555 (2005).
[9] S. J. Pearton, W. H. Heo, M. Ivill, D. P. Norton, and T. Steiner, Semicond. Sci. Technol. **19**, R59 (2004).
[10] T. Dietl, H. Ohno, F. Matsukura, J. Cibert, and D. Ferrand, Science **287**, 1019 (2000).
[11] K. Sato and H. Katayama-Yoshida, Semicond. Sci. Technol. **17**, 367 (2002).
[12] Z. Jin, T. Fukumura, M. Kawasaki, K. Ando, H. Saito, T. Sekiguchi, Y. Z. Yoo, M. Murakami, Y. Matsumoto, T. Hasegawa, and H. Koinuma, Appl. Phys. Lett. **78**, 3824 (2001).
[13] K. Ueda, H. Tabata, and T. Kawai, Appl. Phys. Lett. **79**, 988 (2001).
[14] W. Jung, S.-J. An, G.-C. Yi, C. U. Jung, S.-I. Lee, and S. Cho, Appl. Phys. Lett. **80**, 4561 (2002).
[15] P. Sharma, A. Gupta, K. V. Rao, F. J. Owens, R. Sharma, R. Ahuja, J. M. O. Guillen, B. Johansson, and G. A. Gehring, Nature Mater. **2**, 673 (2003).
[16] D. P. Norton, S. J. Pearton, A. F. Hebard, N. Theodoropoulou, L. A. Boatner, and R. G. Wilson, Appl. Phys. Lett. **82**, 239 (2003).
[17] S. Ramachandran, A. Tiwari, and J. Narayan, Appl. Phys. Lett. **84**, 5255 (2004).
[18] J. M. Baik and J.-L. Lee, Adv. Mater. **17**, 2745 (2005).
[19] O. D. Jayakumar, I. K. Gopalakrishnan, and S. K. Kulshreshtha, Adv. Mater. **18**, 1857 (2006).
[20] X. Wang, J. Xu, B. Zhang, H. Yu, J. Wang, X. Zhang, J. Yu, and Q. Li, Adv. Mater. **18**, 2476 (2006).
[21] T. Fukumura, Z. Jin, M. Kawasaki, T. Shono, T. Hasegawa, S. Koshihara, and H. Koinuma, Appl. Phys. Lett. **78**, 958 (2001).
[22] S. W. Yoon, S.-B. Cho, S. C. We, S. Yoon, B. J. Suh, H. K. Song, and Y. J. Shin, J. Appl. Phys. **93**, 7879 (2003).
[23] S. S. Kim, J. H. Moon, B.-T. Lee, O. S. Song, and J. H. Je, J. Appl. Phys. **95**, 454 (2004).
[24] S. Kolesnik, B. Dabrowski, and J. Mais, J. Appl. Phys. **95**, 2582 (2004).
[25] M. Bouloudenine, N. Viart, S. Colis, J. Kortus, and A. Dinia, Appl. Phys. Lett. **87**, 052501 (2005).
[26] J. H. Kim, H. Kim, D. Kim, Y. E. Ihm, and W. K. Choo, J. Appl. Phys. **92**, 6066 (2002).
[27] D. P. Norton, M. E. Overberg, S. J. Pearton, K. Pruessner, J. D. Budai, L. A. Boatner, M. F. Chisholm, J. S. Lee, Z. G. Khim, Y. D. Park, and R. G. Wilson, Appl. Phys. Lett. **83**, 5488 (2003).
[28] J. H. Park, M. G. Kim, H. M. Jang, S. Ryu, and Y. M. Kim, Appl. Phys. Lett. **84**, 1388 (2004).
[29] K. Ando, H. Saito, Z. Jin, T. Fukumura, M. Kawasaki, Y. Matsumoto, and H. Koinuma, J. Appl. Phys. **89**, 7284 (2001).
[30] H. J. Lee, S. Y. Jeong, C. R. Cho, and C. H. Park, Appl. Phys. Lett. **81**, 4020 (2002).
[31] K. Rode, A. Anane, R. Mattana, J.-P. Contour, O. Durand, and R. Lebourgeois, J. Appl. Phys. **93**, 7676 (2003).
[32] D. A. Schwartz and D. R. Gamelin, Adv. Mater. **16**, 2115 (2004).
[33] N. Khare, M. J. Kappers, M. Wei, M. G. Blamire, and J. L. MacManus-Driscoll, Adv. Mater. **18**, 1449 (2006).
[34] M. H. F. Sluiter, Y. Kawazoe, P. Sharma, A. Inoue, A. R. Raju, C. Rout, and U. V. Waghmare, Phys. Rev. Lett. **94**, 187204 (2005).
[35] K. R. Kittilstved, D. A. Schwartz, A. C. Tuan, S. M. Heald, S. A. Chambers, and D. R. Gamelin, Phys. Rev. Lett. **97**, 037203 (2006).
[36] J. Alaria, H. Bieber, S. Colis, G. Schmerber, and A. Dinia, Appl. Phys. Lett. **88**, 112503 (2006).
[37] X. C. Liu, E. W. Shi, Z. Z. Chen, H. W. Zhang, B. Xiao, and L. X. Song, Appl. Phys. Lett. **88**, 252503 (2006).
[38] T. Zhang, L. X. Song, Z. Z. Chen, E. W. Shi, L. X. Chao, and H. W. Zhang, Appl. Phys. Lett. **89**, 172502 (2006).
[39] M. Venkatesan, P. Stamenov, L. S. Dorneles, R. D. Gunning, B. Bernoux, and J. M. D. Coey, Appl. Phys. Lett. **90**, 242508 (2007).
[40] Z. Yang, J. L. Liu, M. Biasini, and W. P. Beyermann, Appl. Phys. Lett. **92**, 042111 (2008).
[41] K. R. Kittilstved, N. S. Norberg, and D. R. Gamelin, Phys. Rev. Lett. **94**, 147209 (2005).
[42] Z. B. Gu, M. H. Lu, J. Wang, D. Wu, S. T. Zhang, X. K. Meng, Y. Y. Zhu, S. N. Zhu, Y. F. Chen, and X. Q. Pan, Appl. Phys. Lett. **88**, 082111 (2006).
[43] H. Y. Xu, Y. C. Liu, C. S. Xu, Y. X. Liu, C. L. Shao, and R. Mu, Appl. Phys. Lett. **88**, 242502 (2006).
[44] W. Yan, Z. Sun, Q. Liu, Z. Li, T. Shi, F. Wang, Z. Qi, G. Zhang, S. Wei, H. Zhang, and Z. Chen, Appl. Phys. Lett. **90**, 242509 (2007).
[45] Q. Wan, Appl. Phys. Lett. **89**, 082515 (2006).
[46] M. Ivill, S. J. Pearton, Y. W. Heo, J. Kelly, A. F. Hebard, and D. P. Norton, J. Appl. Phys. **101**, 123909 (2007).
[47] K. Lord, T. M. Williams, D. Hunter, K. Zhang, J. Dadson, and A. K. Pradhan, Appl. Phys. Lett. **88**, 262105 (2006).
[48] S. Lee, D. Y. Kim, Y. Shon, and C. S. Yoon, Appl. Phys. Lett. **89**, 022120 (2006).
[49] Y. Z. Peng, T. Liew, T. C. Chong, C. W. An, and W. D. Song, Appl. Phys. Lett. **88**, 192110 (2006).
[50] Q. Xu, L. Hartmann, H. Schmidt, H. Hochmuth, M. Lorenz, R. Schmidt-Grund, C. Sturm, D. Spemann, and M. Grundmann, Phys. Rev. B **73**, 205342 (2006).
[51] Q. Xu, L. Hartmann, H. Schmidt, H. Hochmuth, M. Lorenz, R. Schmidt-Grund, C. Sturm, D. Spemann, M. Grundmann, and Y. Liu, J. Appl. Phys. **101**, 063918 (2007).
[52] W. Shim, K. Lee, W. Lee, K. A. Jeon, S. Y. Lee, and M. H. Jung, J. Appl. Phys. **101**, 123908 (2007).
[53] H. Pan, J. B. Yi, L. Shen, R. Q. Wu, J. H. Yang, J. Y. Lin, Y. P. Feng, J. Ding, L. H. Van, and J. H. Yin, Phys. Rev. Lett. **99**, 127201 (2007).
[54] Z. Yang, D. C. Look, and J. L. Liu (unpublished).
[55] J. M. D. Coey, M. Venkatesan, and C. B. Fitzgerald, Nature Mater. **4**, 173 (2005).
[56] P. Sati, R. Hayn, R. Kuzian, S. Régnier, S. Schäfer, A. Stepanov, C. Morhain, C. Deparis, M. Laügt, M. Goiran, and Z. Golacki, Phys. Rev. Lett. **96**, 017203 (2006).
[57] M. Venkatesan, C. B. Fitzgerald, J. G. Lunnery, and J. M. D. Coey, Phys. Rev. Lett. **93**, 177206 (2004).
[58] C. Song, K. W. Geng, F. Zeng, X. B. Wang, Y. X. Sheng, F. Pan, Y. N. Xie, T. Liu, T. T. Zhou, and Z. Fan, Phys. Rev. B **73**, 024405 (2006).
[59] A. Zukova, A. Teiserskis, S. V. Dijken, Y. K. Gun'Ko, and V. Kazlauskiene, Appl. Phys. Lett. **89**, 232503 (2006).
[60] S. B. Ogale, R. J. Choudhary, J. P. Buban, S. E. Lofland, S. R. Shinde, S. N. Kale, V. N. Kulkarni, J. Higgins, C. Lanci, J. R. Simpson, N. D. Browning, S. D. Sarma, H. D. Drew, R. L. Greene, and T. Venkatesan, Phys. Rev. Lett. **91**, 077205 (2003).
[61] T. Andrearczyk, J. Jaroszyński, G. Grabecki, T. Dietl, T. Fukumura, and M. Kawasaki, Phys. Rev. B **72**, 121309(R) (2005).
[62] J. Wang, Z. Gu, M. Lu, D. Wu, C. Yuan, S. Zhang, Y. Chen, S. Zhu, and Y. Zhu, Appl. Phys. Lett. **88**, 252110 (2006).
[63] Q. Xu, L. Hartmann, H. Schmidt, H. Hochmuth, M. Lorenz, R. Schmidt-Grund, D. Spemann, and M. Grundmann, J. Appl. Phys. **100**, 013904 (2006).
[64] M. Gacic, G. Jakob, C. Herbort, and H. Adrian, Phys. Rev. B **75**, 205206 (2007).
[65] F. Reuss, S. Frank, C. Kirchner, R. Kling, Th. Gruber, and A. Waag, Appl. Phys. Lett. **87**, 112104 (2005).
[66] R. P. Khosla and J. R. Fischer, Phys. Rev. B **2**, 4084 (1970).
[67] Z. Yang, Z. Zuo, Y. Pu, W. P. Beyermann, J. Shi, and J. L. Liu, (unpublished).
[68] R. C. O'Handley, *Modern Magnetic Materials* (Wiley, New York, 2000), pp. 570–573.
[69] I. A. Campbell and A. Fert, *Transport Properties of Ferromagnets*, Ferromagnetic Materials Vol. 3, edited by E. P. Wohlfarth (North-Holland, Amsterdam, 1982), Ch. 9, pp. 766–800.